

Dissipative structures in a nonlinear dynamo

Andrew D. Gilbert,^a Yannick Ponty^b
and Vladislav Zheligovsky^c

^a*Mathematics Research Institute, University of Exeter, U.K.*

^b*Observatoire de la Côte d’Azur, Nice, France.*

^c*International Institute of Earthquake Prediction Theory
and Mathematical Geophysics, Moscow, Russia.*

Abstract

This paper considers magnetic field generation by a fluid flow in a system referred to as the Archontis dynamo: a steady nonlinear magnetohydrodynamic (MHD) state is driven by a prescribed body force. The field and flow become almost equal and dissipation is concentrated in cigar-like structures centred on straight-line separatrices. Numerical scaling laws for energy and dissipation are given that extend previous calculations to smaller diffusivities. The symmetries of the dynamo are set out, together with their implications for the structure of field and flow along the separatrices. The scaling of the cigar-like dissipative regions, as the square root of the diffusivities, is explained by approximations near the separatrices. Rigorous results on the existence and smoothness of solutions to the steady, forced MHD equations are given.

Key words: fast dynamo, Archontis dynamo, dissipation, symmetry

1 Introduction

Much is known about fast dynamo action: the rapid growth of magnetic fields at high magnetic Reynolds number in fluid flows with chaotic streamlines, but the mechanisms for the dynamical saturation of such fields remain poorly understood. In many cases when the growing field equilibrates by modifying the fluid motion, the effect is to switch off the chaotic stretching in the flow, as measured for example by a reduction in the finite-time Liapunov exponents (e.g., Cattaneo, Hughes & Kim, 1996; Zienicke, Politano & Pouquet, 1998). What is left is a fluid threaded by a magnetic field which resists stretching

and so suppresses overturning fluid motions, but supports elastic wave-like motions, essentially Alfvén waves with coupled field and flow (e.g., Courvoisier, Hughes & Proctor, 2010). The final state of many simulations shows apparently chaotic behaviour in space and time, suggestive of an attractor of moderate or high dimension, although because of the three-dimensionality of MHD systems little can be done to explore its properties, for example the fractal dimension or spectrum of Liapunov exponents.

Although this appears to be the outcome of many simulations, as far as they can be run, there are some intriguing examples where a further phase of evolution takes place: the magnetic field and flow align, depleting the nonlinear terms, and both fields evolve to a steady (or very slowly evolving) state. The key point is that in unforced, ideal magnetohydrodynamics (see equations (2.1–2.3) below with $\nu = \eta = 0$ and $\mathbf{f} = 0$) any state with $\mathbf{u} = \pm \mathbf{b}$ is an exact steady solution. The remarkable fact that simulations of forced, non-ideal MHD turbulence could evolve to something very close to such a state was first observed by Archontis (2000) in his thesis, and published in Dorch & Archontis (2004) (hence referred to as DA), and Archontis, Dorch & Nordlund (2007). These simulations use a compressible code with a Kolmogorov forcing function, (2.4) below, first used as the form of a flow for simulations of fast, kinematic dynamo action by Galloway & Proctor (1992). Subsequently Cameron & Galloway (2006a) undertook incompressible simulations of the same system as Archontis, and pushed up the fluid and magnetic Reynolds numbers; our work is linked closely to this paper, which we refer to as CG in what follows.

What these authors found was that, starting with a forced fluid flow and a seed magnetic field, the growing magnetic field initially equilibrates in rough equipartition with the velocity field, in a messy, chaotic time-dependent state. However during this state, there is a slow but persistent exponential growth in the average alignment of the \mathbf{u} and \mathbf{b} vectors, as measured by the cross-helicity. This process of alignment continues until there takes place a sudden increase in the fluid and magnetic energies, and both fields tend to a steady state of almost perfect alignment, discrepancies being controlled by the weak dissipation and the forcing. In fact since any solution $\mathbf{u} = \pm \mathbf{b}$ is a neutrally stable solution of the ideal problem (Friedlander & Vishik, 1995), the solution that is selected must depend delicately on balances involving these subdominant diffusive and forcing effects. We note that some alignment of field and flow has been noted in many other MHD flows, for example see Dobrowolny, Mangeney & Veltri (1980), Pouquet, Meneguzzi & Frisch (1986), Mason, Cattaneo & Boldyrev (2006) and references therein, but of a less dramatic nature.

This observation of dynamo saturation in a steady state with such a high degree of alignment was a new phenomenon: CG refer to the saturated state as the ‘Archontis dynamo’, though we prefer the term ‘Archontis saturation

mechanism'. CG observed this aligned state as a solution branch over a wide range of magnetic and fluid Reynolds numbers (taking the magnetic Prandtl number to be unity in much of their work). Further developments include the development of bursts of rapid time dependence after some time in the steady state, in the study Archontis, Dorch & Nordlund (2007). However this appears only to occur in the compressible case, as it has not been seen by CG nor in our simulations; we will therefore not discuss this further. Cameron & Galloway (2006b) also find slow time-dependent evolution of the saturated state for the Kolmogorov forcing with magnetic Prandtl number $\text{Pr} = \nu/\eta$ not equal to unity, and for more general spatially periodic steady forcings. In all cases though, the field and flow settle into a state of very close alignment, even if they then evolve on a slow time scale.

The focus of the present paper is to understand more about the structure of the steady saturated state for the Kolmogorov forcing and unit magnetic Prandtl number Pr , with a particular focus on the regions where dissipation occurs and on rigorous results on existence and smoothness. DA and CG find a complex geometrical picture for the field and flow and identify these regions of high dissipation: they are localised along straight-line separatrices that join a family of stagnation points; similar structures are found in the 1:1:1 ABC flow (Dombre *et al.*, 1986). These are found to have a width scaling as $\sqrt{\varepsilon}$ where ε is a dimensionless measure of the diffusivity, and one of our aims is to understand this power law.

We set up the governing equations in §2 and extend the solution branch to yet smaller values of the diffusivity ε by means of large scale simulations in §3. In §4 we then classify the symmetries of the Kolmogorov forcing, which are preserved by the nonlinear, saturated field and flow. These symmetries are the reason for the presence of the non-generic straight line separatrices that join stagnation points in the flow and field, and they constrain the local flow: it is in these regions that dissipation is strongest. We plot the local structure of fields along the separatrix from $(0, 0, 0)$ to (π, π, π) in §5. We determine the effects of diffusion by setting up PDEs for the advection of field as it enters the dissipative regions in §6 and use these to justify the order $\sqrt{\varepsilon}$ scaling for the cigar widths found in CG. We then proceed with a formal mathematical investigation of the existence of steady-state solutions to the MHD problem at hand and bounds for them in various function spaces in §§7–9. The reader should note that these sections use functional analysis and so have a different flavour from the earlier ones. Finally §10 offers concluding discussion.

2 Governing equations

We begin with the dimensional equations for incompressible MHD, in the form

$$\partial_t \mathbf{u} + \mathbf{u} \cdot \nabla \mathbf{u} = \mathbf{b} \cdot \nabla \mathbf{b} - \nabla p + \nu \nabla^2 \mathbf{u} + \mathbf{f}, \quad (2.1)$$

$$\partial_t \mathbf{b} + \mathbf{u} \cdot \nabla \mathbf{b} = \mathbf{b} \cdot \nabla \mathbf{u} + \eta \nabla^2 \mathbf{b}, \quad (2.2)$$

$$\nabla \cdot \mathbf{u} = \nabla \cdot \mathbf{b} = 0, \quad (2.3)$$

where ν and η are the kinematic viscosity and magnetic diffusivity. We take \mathbf{f} to be a steady force of magnitude \mathcal{F} acting on a length scale \mathcal{L} . We will consider the *Kolmogorov forcing* $\mathbf{f} = \mathcal{F} \mathbf{f}^*(\mathbf{r}/\mathcal{L})$, whose dimensionless form is given by

$$\mathbf{f}^*(\mathbf{r}) = (\sin z, \sin x, \sin y). \quad (2.4)$$

In non-dimensionalising we have only the parameters $\{\mathcal{L}, \mathcal{F}, \nu, \eta\}$, together with the form (2.4) of the forcing function. From these we can define a magnetic Prandtl number and a Grashof number as in similar forced flow problems (see, e.g., Childress, Kerswell & Gilbert, 2001) by

$$\text{Pr} = \nu/\eta, \quad \text{Gr} = \mathcal{F} \mathcal{L}^3 / \nu^2 \equiv \varepsilon^{-1}. \quad (2.5)$$

We have as diagnostics the Reynolds number and magnetic Reynolds number given by

$$\text{Re} = \mathcal{L} \|\mathbf{u}\| / \nu, \quad \text{Rm} = \mathcal{L} \|\mathbf{u}\| / \eta, \quad (2.6)$$

where $\|\mathbf{u}\|$ is a measure of the fluid velocity at a given time, for example the L^2 norm, taken as the root-mean-square value, averaged over the periodicity box. We rescale as

$$\mathbf{u} = \mathcal{U} \mathbf{u}^*, \quad \mathbf{b} = \mathcal{U} \mathbf{b}^*, \quad t = (\mathcal{L}/\mathcal{U}) t^*, \quad \mathbf{r} = \mathcal{L} \mathbf{r}^*, \quad \mathbf{f} = \mathcal{F} \mathbf{f}^*, \quad p = \mathcal{U}^2 p^*, \quad (2.7)$$

with the choice of velocity scale

$$\mathcal{U} = \mathcal{F} \mathcal{L}^2 / \nu. \quad (2.8)$$

This yields the non-dimensional formulation, dropping the stars, as

$$\partial_t \mathbf{u} + \mathbf{u} \cdot \nabla \mathbf{u} = \mathbf{b} \cdot \nabla \mathbf{b} - \nabla p + \varepsilon \nabla^2 \mathbf{u} + \varepsilon \mathbf{f}, \quad (2.9)$$

$$\partial_t \mathbf{b} + \mathbf{u} \cdot \nabla \mathbf{b} = \mathbf{b} \cdot \nabla \mathbf{u} + \varepsilon \text{Pr}^{-1} \nabla^2 \mathbf{b}, \quad (2.10)$$

$$\nabla \cdot \mathbf{u} = \nabla \cdot \mathbf{b} = 0, \quad (2.11)$$

with \mathbf{f} given in (2.4) and the only parameters specified are $\{\varepsilon, \text{Pr}\}$. The corresponding Reynolds and magnetic Reynolds numbers are

$$\text{Re} = \varepsilon^{-1} \|\mathbf{u}\|, \quad \text{Rm} = \varepsilon^{-1} \text{Pr} \|\mathbf{u}\|. \quad (2.12)$$

We refer to ε^{-1} as the Grashof number Gr and will be interested in the inviscid limit $\varepsilon \rightarrow 0$. The Reynolds number and magnetic Reynolds number are diagnostics depending on the flow regime realised.¹ Indeed, they change greatly during the saturation process, when the fields align and $\|\mathbf{u}\|$, $\|\mathbf{b}\|$ increase significantly. As in CG, the governing equations may be written in a more symmetrical form in terms of Elsasser variables

$$\mathbf{\Lambda}_{\pm} = \mathbf{u} \pm \mathbf{b}, \quad (2.13)$$

which gives, for $\text{Pr} = 1$,

$$\partial_t \mathbf{\Lambda}_+ + \mathbf{\Lambda}_- \cdot \nabla \mathbf{\Lambda}_+ = -\nabla p + \varepsilon \nabla^2 \mathbf{\Lambda}_+ + \varepsilon \mathbf{f}, \quad (2.14)$$

$$\partial_t \mathbf{\Lambda}_- + \mathbf{\Lambda}_+ \cdot \nabla \mathbf{\Lambda}_- = -\nabla p + \varepsilon \nabla^2 \mathbf{\Lambda}_- + \varepsilon \mathbf{f}, \quad (2.15)$$

$$\nabla \cdot \mathbf{\Lambda}_+ = \nabla \cdot \mathbf{\Lambda}_- = 0. \quad (2.16)$$

3 Numerical results

We undertook a number of runs to investigate the structure of the steady, equilibrated Archontis dynamo for $\text{Pr} = 1$ and values of ε down to 10^{-4} in the $(2\pi)^3$ periodic domain \mathbb{T}^3 . The steady solutions were found by following the solution branch: that is taking the output from a run with a given value of ε and using it as the initial condition for a run with a reduced value of ε . This establishes the Archontis dynamo as a robust local attractor, in the range of ε used, in agreement with DA and CG. Whether it is a global attractor over some or all sufficiently small values of ε remains unknown, and extremely difficult to address in view of the long transients that may occur. Our runs were undertaken with a pseudo-spectral code using N^3 modes with $N = 128$ for $\varepsilon = 0.02$ and 0.01 , $N = 256$ for $\varepsilon = 10^{-3}$, and $N = 512$ for $\varepsilon = 10^{-4}$. There were other, less well resolved runs with $N = 128$ for $\varepsilon = 10^{-3}$ and $N = 256$ for $\varepsilon = 10^{-4}$, which we refer to below as our ‘testing simulations’. For comparison, CG go down to $\varepsilon = 1.25 \times 10^{-3}$ in their study, with resolution 128^3 . Our results thus extend theirs by a little over a decade, and in this section we present measures of the magnetic field and flow in the equilibrated state.

Numerical values are given in table 1 and plotted in figure 1. Panel 1(a) shows the kinetic and magnetic energies in the equilibrated state, given by

$$E_K = \int_{\mathbb{T}^3} \frac{1}{2} |\mathbf{u}|^2 dV, \quad E_M = \int_{\mathbb{T}^3} \frac{1}{2} |\mathbf{b}|^2 dV. \quad (3.1)$$

¹ Our formulation is equivalent to DA/CG, but our terminology is a little different. For example CG use the parameters $\nu_{\text{CG}} \equiv \varepsilon$ and $\eta_{\text{CG}} \equiv \varepsilon \text{Pr}^{-1}$, which they refer to as the inverse Reynolds and magnetic Reynolds numbers respectively.

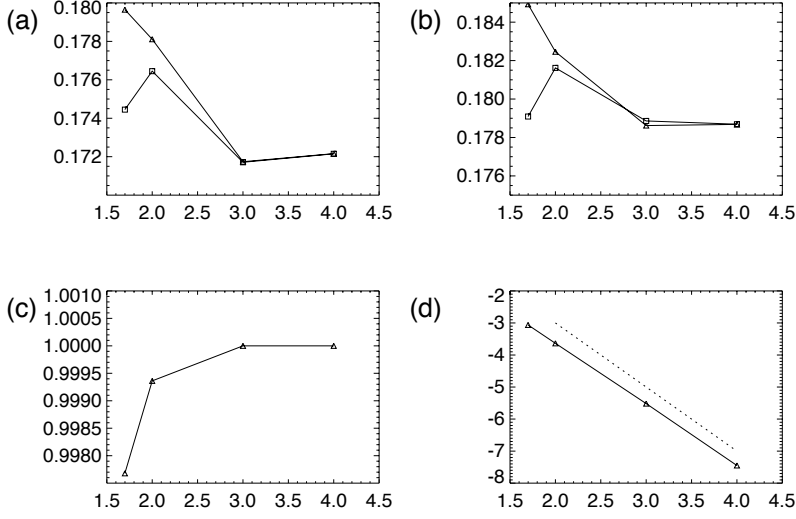


Fig. 1. Numerical results plotted against $\log_{10} \varepsilon^{-1}$. Plotted are (a) kinetic energy E_K (triangles) and magnetic energy E_M (squares), (b) enstrophy Ω_K (triangles) and squared current Ω_M (squares), (c) normalised cross helicity $H_X/(2E_K E_M)$, (d) energy $\log_{10} E_-$ of Λ_- (dotted line gives ε^2 dependence).

ε	N	E_K	E_M	Ω_K	Ω_M	H_X	E_-
0.02	64	0.1797	0.1745	0.1849	0.1791	0.3532	8.685×10^{-4}
0.01	64	0.1781	0.1765	0.1825	0.1816	0.3543	2.313×10^{-4}
0.001	256	0.1717	0.1717	0.1786	0.1789	0.3435	3.04×10^{-6}
0.0001	512	0.1722	0.1722	0.1787	0.1787	0.3443	3.55×10^{-8}

Table 1
Numerical results.

These show an initial decrease with ε (as in CG) but then a slight increase from $\varepsilon = 10^{-3}$ to $\varepsilon = 10^{-4}$: this is quite small bearing in mind the scale on the vertical axis, but appears to be real as it is borne out in our test simulations. In all these runs $E_K > E_M$ though this is not apparent from the numbers in table 1 nor in panel 1(a). Panel 1(b) shows the enstrophy and integrated squared current, defined by

$$\Omega_K = \int_{\mathbb{T}^3} \frac{1}{2} |\nabla \times \mathbf{u}|^2 dV, \quad \Omega_M = \int_{\mathbb{T}^3} \frac{1}{2} |\nabla \times \mathbf{b}|^2 dV. \quad (3.2)$$

The total dissipation is given by $2\varepsilon\Omega_K + 2\varepsilon\Omega_M$ and this tends to zero as $O(\varepsilon)$, as does the input of mechanical energy. Panel 1(c) shows the cross helicity

$$H_X = \int_{\mathbb{T}^3} \mathbf{u} \cdot \mathbf{b} dV \quad (3.3)$$

in normalised form, which rapidly tends to its theoretical upper bound of

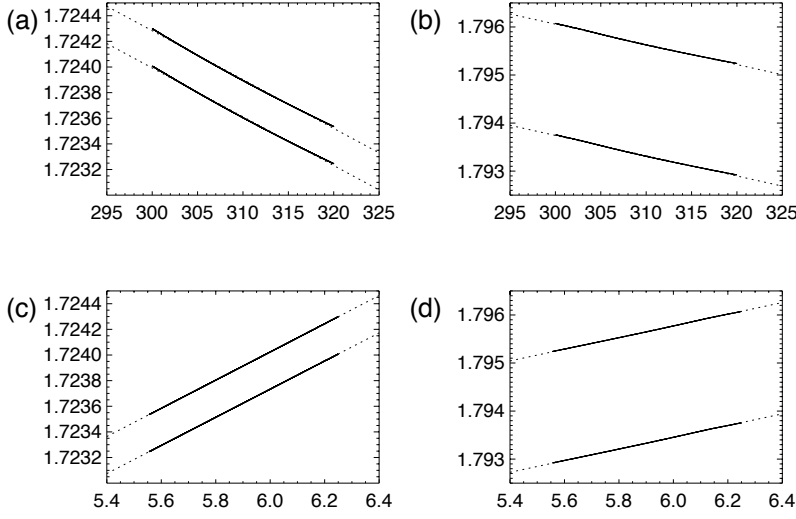


Fig. 2. Numerical results for the case $\varepsilon = 10^{-3}$ with $N = 256$. Plotted are (a) $10E_K$ (upper) and $10E_M$ (lower), (b) $10\Omega_K$ (lower) and $10\Omega_M$ (upper), against $t/10$. (c,d) are the same but plotted against $10^4/(t-1400)$. In each panel dotted lines are linear fits.

unity, within the accuracy of our simulations, indicating the strong alignment of field as $\varepsilon \rightarrow 0$. Finally panel 1(d) shows the energy in the $\mathbf{\Lambda}_-$ Elsasser variable, where

$$E_{\pm} = \int_V \frac{1}{2} |\mathbf{\Lambda}_{\pm}|^2 dV \equiv E_K + E_M \pm H_X. \quad (3.4)$$

This shows a rapid decrease to zero as $\varepsilon \rightarrow 0$, with $E_- \propto \varepsilon^2$ (dotted line) in agreement with the discussion in CG and below.

In panel 1(b) it is notable that the two curves, for enstrophy and total current squared, cross between $\varepsilon = 0.01$ and 0.001 . The enstrophy Ω_K is a little smaller than Ω_M for $\varepsilon = 10^{-3}$ and in fact is also for 10^{-4} and in our test simulations, making us confident that this is a real effect. This opens up the question of how we measure these quantities, since the rate of evolution of the state becomes extremely slow for small ε . Figure 2(a,b) shows E_K , E_M , Ω_K and Ω_M as functions of time for the case $\varepsilon = 10^{-3}$ and $N = 256$: comparison with linear fits (dotted) shows clear curvature, as one might expect, but also highlights the slow evolution. The slow evolution suggests neutral stability of the final state, and an expansion for any quantity in the form

$$A = A_0 + A_1 t^{-1} + A_2 t^{-2} + \dots. \quad (3.5)$$

Although asymptotically the origin of time does not matter, we found it helpful to choose an origin of time t_0 (once per run) so as to obtain the best linear fit

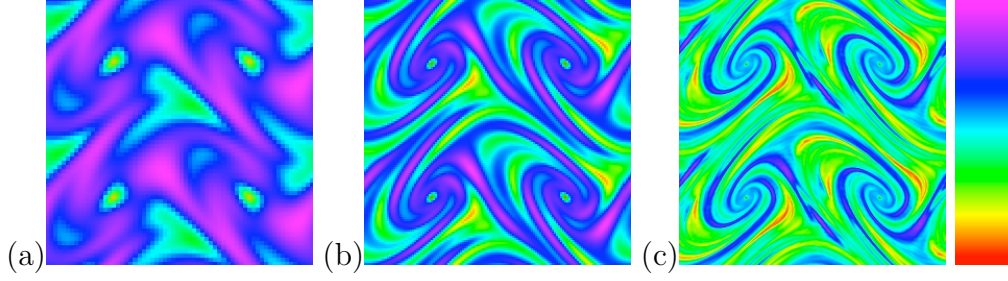


Fig. 3. Cross sections showing $|\mathbf{\Lambda}_-|$ in the (x, y) -plane for $z = \pi/2$. In (a) $\varepsilon = 10^{-2}$, (b) 10^{-3} and (c) 10^{-4} and the colour scale shown runs from zero (bottom) to (a) 0.031, (b) 0.0041 and (c) 0.00058 (top).

for quantities in the form

$$A \simeq A_0 + A_1(t - t_0)^{-1} \quad (3.6)$$

We then use an estimate of the limiting value as A_0 ; for example see figure 2 (c,d). This was done for all the results in table 1.

One of the aims of this paper is to focus on dissipative regions in the system: these occur along a series of straight line separatrices (DA/CG) and in figure 3, we show colour plots of $|\mathbf{\Lambda}_-|$ for a range of diffusivities. Clearly seen in each case, but especially in (c) at the smallest ε , are cross sections of spiralling field, centred on the separatrices, where small scales are generated with consequently enhanced diffusion.

4 Symmetries

We have seen that the dissipation tends to concentrate in cigar shaped regions, with one extending from $(0, 0, 0)$ to the stagnation points at $\pm(\pi, \pi, \pi)$. The reason these straight line separatrices are robust structures is linked to the symmetries of the forcing (2.4) and also applies to the kinematic dynamo study by Galloway & Proctor (1992) of the Kolmogorov flow

$$\mathbf{u}_{\text{Kol}}(\mathbf{r}) = (\sin z, \sin x, \sin y). \quad (4.1)$$

These symmetries turn out to be preserved by the solution (\mathbf{u}, \mathbf{b}) in the non-linear regime: there is no symmetry breaking. The forcing (2.4) is 2π -periodic in each coordinate: we only consider symmetries up to this periodicity (and that do not reverse time). Note first that any map T maps a vector field \mathbf{u} according to

$$(T\mathbf{u})(\mathbf{r}) = \mathbf{J}_T \cdot \mathbf{u}(T^{-1}\mathbf{r}), \quad \mathbf{J}_T = \partial\mathbf{r}/\partial T^{-1}\mathbf{r}. \quad (4.2)$$

It is then easily checked that the forcing \mathbf{f} in (2.4) is preserved by the following 12 orientation-preserving symmetries, with $\det \mathbf{J} = 1$, which form the group A_4 of even permutations of 4 objects, or the symmetry group of the tetrahedron,

$$\begin{aligned}
i(\mathbf{r}) &= (x, y, z), & a^2(\mathbf{r}) &= (-x, \pi - y, z + \pi), \\
b^2(\mathbf{r}) &= (x + \pi, -y, \pi - z), & c^2(\mathbf{r}) &= (\pi - x, y + \pi, -z), \\
d(\mathbf{r}) &= (z, x, y), & d^2(\mathbf{r}) &= (y, z, x), \\
e(\mathbf{r}) &= (-z, \pi - x, y + \pi), & e^2(\mathbf{r}) &= (\pi - y, z + \pi, -x), \\
f(\mathbf{r}) &= (z + \pi, -x, \pi - y), & f^2(\mathbf{r}) &= (-y, \pi - z, x + \pi), \\
g(\mathbf{r}) &= (\pi - z, x + \pi, -y), & g^2(\mathbf{r}) &= (y + \pi, -z, \pi - x).
\end{aligned} \tag{4.3}$$

These also form a subgroup of the group of 24 symmetries of the 1:1:1 ABC flow (Arnold & Korkina, 1983; Dombre *et al.*, 1986), and the above follows the notation in Gilbert (1992). The symmetries all commute with the inversion symmetry $j(\mathbf{r}) = (-x, -y, -z)$ and so the full symmetry group of the forcing \mathbf{f} is the direct product $A_4 \times \mathbb{Z}_2$.

5 Flow and field on the separatrices

The above symmetries constrain the behaviour of the magnetic field and flow on the separatrices. Take, for definiteness, the separatrix joining $(0, 0, 0)$ to (π, π, π) and call this the ‘main separatrix’ for brevity. Because of the symmetries d and d^2 in (4.3) there is a three-fold rotational symmetry about this separatrix, as seen in DA/CG, and any vector field on the separatrix can only point along the separatrix. We may introduce rotated Cartesian coordinates via

$$\begin{pmatrix} \mu \\ \chi \\ \zeta \end{pmatrix} = \begin{pmatrix} 1/\sqrt{2} & -1/\sqrt{2} & 0 \\ 1/\sqrt{6} & 1/\sqrt{6} & -2/\sqrt{6} \\ 1/\sqrt{3} & 1/\sqrt{3} & 1/\sqrt{3} \end{pmatrix} \begin{pmatrix} x \\ y \\ z \end{pmatrix}, \tag{5.1}$$

with ζ along the separatrix. From there we may further define cylindrical polar coordinates (ρ, θ, ζ) , whose axis is ζ along the separatrix with $\mu = \rho \cos \theta$ and $\chi = \rho \sin \theta$.

Our aim now is to investigate more of the behaviour of the flow near to the separatrix, in the saturated regime. However to fix ideas and establish a benchmark, we consider first the Kolmogorov flow \mathbf{u}_{Kol} in (4.1). For this flow it can be shown that on the main separatrix motion is governed by

$$\dot{\zeta} = \sqrt{3} \sin(\zeta/\sqrt{3}), \quad \mu = \nu = 0, \tag{5.2}$$

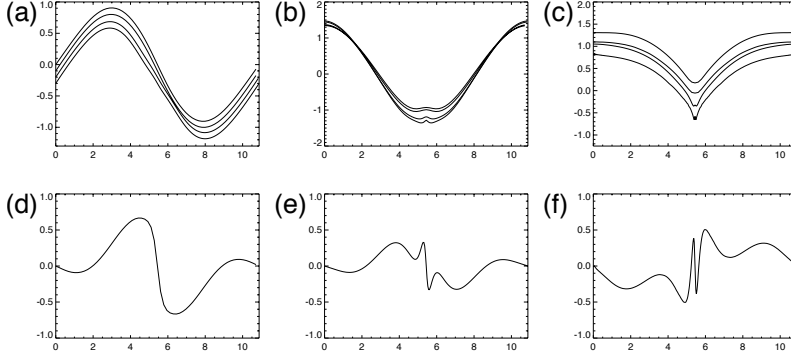


Fig. 4. Plot of components of fields against ζ for runs with $\varepsilon = 0.02, 0.01, 10^{-3}$ and 10^{-4} for (a) the field $\mathbf{\Lambda}_+$, reading down the curves (separated by adding 0, -0.1 , -0.2 , etc.), (b) the field $\nabla \times \mathbf{\Lambda}_+$, reading down the curves (c) the field $\varepsilon^{-1/2} \nabla \times \mathbf{\Lambda}_+$, reading down the curves (separated by adding 0, -0.25 , -0.5 , etc.) (d,e,f) the field $\varepsilon^{-1} \mathbf{\Lambda}_-$ for ε equal to (d) 0.01, (e) 10^{-3} and (f) 10^{-4} .

with solution

$$\zeta = \sqrt{3}(\pi - \cos^{-1} \tanh t). \quad (5.3)$$

Here ζ tends to zero as $t \rightarrow -\infty$ and to $\sqrt{3}\pi$ as $t \rightarrow \infty$. Near to the separatrix, the radial coordinate $\rho \ll 1$ and the flow field may be expanded in powers of ρ . In view of the three-fold rotational symmetry, the flow \mathbf{u} is axisymmetric about the main separatrix $\rho = 0$ at leading order and streamlines are given by

$$\dot{\rho} = -s'(\zeta)\rho + O(\rho^2), \quad \dot{\theta} = \Omega(\zeta) + O(\rho), \quad \dot{\zeta} = 2s(\zeta) + O(\rho^2), \quad (5.4)$$

with

$$2s_{\text{Kol}}(\zeta) = \sqrt{3} \sin(\zeta/\sqrt{3}), \quad 2\Omega_{\text{Kol}}(\zeta) = \sqrt{3} \cos(\zeta/\sqrt{3}). \quad (5.5)$$

Trajectories spiral in for $\zeta \simeq 0$ and spiral out for $\zeta \simeq \sqrt{3}\pi$. On the separatrix itself $\mathbf{u} = (0, 0, 2s(\zeta))$ and $\nabla \times \mathbf{u} = (0, 0, 2\Omega(\zeta))$, directed along the axis.

Now in the nonlinear, equilibrated regime, the symmetries of the system are observed to be preserved and so the motion near and along the separatrix is given by (5.4) for some functions $s(\zeta)$ and $\Omega(\zeta)$. These functions characterise aspects of the nonlinear saturation on the separatrices and so of the spiral dissipative structures that form there, visible in figure 3. We can measure the equivalent functions for any field, and in our runs we find that the traces for $2\mathbf{u}$, $2\mathbf{b}$ and $\mathbf{\Lambda}_+$ are identical to graphical accuracy. In figure 4(a) we show the components of $\mathbf{\Lambda}_+$ along the separatrix (separated by constants). This figure in fact depicts two separatrices, the main separatrix from $(0, 0, 0)$ to (π, π, π) and the next one that continues to $(2\pi, 2\pi, 2\pi)$, with $0 \leq \zeta \leq 2\sqrt{3}\pi$. The components of $\mathbf{\Lambda}_+$ show a sinusoidal form in keeping with the property of the equilibrated fields noted by CG, namely

$$2\mathbf{u} \simeq 2\mathbf{b} \simeq \mathbf{\Lambda}_+ \simeq \mathbf{u}_{\text{Kol}} \quad (5.6)$$

and there is only slight steepening at (π, π, π) as ϵ is reduced. Panel 4(b) shows

traces of the components of $\nabla \times \mathbf{\Lambda}_+$ with clear cosine form, in keeping with (5.6) and (5.5) but of somewhat enhanced amplitude, and with evidence of some finer scale structure near (π, π, π) . These indicate that the approximation (5.6) is reasonable for the leading order fields on the separatrices.

The picture is naturally more complicated for the $\mathbf{\Lambda}_-$ field, which tends to zero in the limit of small ε . Panels 4(d,e,f) plot the components of $\varepsilon^{-1}\mathbf{\Lambda}_-$ along the separatrix: there is clear evidence of finer scale oscillations emerging in the limit, but the nature of the limiting distribution is unclear. Panel 4(c) shows the fields $\varepsilon^{-1/2}\nabla \times \mathbf{\Lambda}_-$ (separated by constants). These show the development of a cusp at (π, π, π) , the stagnation point where the two separatrices converge. In conclusion, the field $\mathbf{\Lambda}_-$ on the separatrix scales as $O(\varepsilon)$, but its curl scales as $O(\varepsilon^{1/2})$, giving a natural $O(\varepsilon^{1/2})$ cigar width length scale, confirming results in CG and to be explored further below.

6 Local behaviour and scaling in the cigars

We now have some knowledge of the local structure of the flow and field on the separatrices, in terms of both the general form it must take, namely (5.4), and the actual behaviour for small values of ε in figure 4. The aim of the present section is to derive the dissipative lengthscale of $\sqrt{\varepsilon}$ noted by CG. Of course we are not able to put together a solution that is complete: the dissipative, cigar-like regions process field that is drawn in, in a spiralling fashion, and then churn it out again. A complete picture would involve matching to the outer region, which is a highly three-dimensional problem, beyond what we can do; nonetheless a local picture gives some information.

6.1 Uncurling the induction equation

We start with the formulation in Elsasser variables (2.13–2.16) and for brevity set

$$\mathbf{\Lambda} \equiv \mathbf{\Lambda}_+, \quad \varepsilon \mathbf{\lambda} \equiv \mathbf{\Lambda}_-, \quad p \rightarrow \varepsilon p. \quad (6.1)$$

We assume the key scaling of CG that $\mathbf{\lambda} = O(1)$, at least in the outer region, which means away from the stagnation points and the separatrices. Without approximation, the steady equations are

$$\mathbf{\lambda} \cdot \nabla \mathbf{\Lambda} = -\nabla p + \nabla^2 \mathbf{\Lambda} + \mathbf{f}, \quad (6.2)$$

$$\mathbf{\Lambda} \cdot \nabla \mathbf{\lambda} = -\nabla p + \varepsilon \nabla^2 \mathbf{\lambda} + \mathbf{f}. \quad (6.3)$$

Note that a straightforward estimate of the width of a diffusive layer based on (6.3) would suggest an order ε scaling from balancing $\mathbf{\Lambda} \cdot \nabla \mathbf{\lambda} \sim \varepsilon \nabla^2 \mathbf{\lambda}$, but this

is too small, as it does not take into account the different scales of variation of $\boldsymbol{\lambda}$ along and across the characteristics of $\boldsymbol{\Lambda}$, and the following, more delicate argument is needed.

Subtracting (6.3) from (6.2) gives an equation equivalent to the induction equation (2.10),

$$0 = \nabla \times (\boldsymbol{\lambda} \times \boldsymbol{\Lambda}) + \nabla^2 \boldsymbol{\Lambda} - \varepsilon \nabla^2 \boldsymbol{\lambda}, \quad (6.4)$$

which may be uncurled as

$$\nabla a = \boldsymbol{\lambda} \times \boldsymbol{\Lambda} - \nabla \times \boldsymbol{\Lambda} + \varepsilon \nabla \times \boldsymbol{\lambda}, \quad (6.5)$$

where $a(\mathbf{r})$ is a scalar field. Taking the divergence gives an elliptic equation for a ,

$$\nabla^2 a = \nabla \cdot (\boldsymbol{\lambda} \times \boldsymbol{\Lambda}). \quad (6.6)$$

This development can be pursued further, to obtain a general closed but complicated system of scalar PDEs that link the field and flow to the external forcing, as in Zheligovsky (2009). However our present aims are more limited: we only need that (6.5) is equivalent to two equations,

$$\boldsymbol{\Lambda} \cdot \nabla a = -\boldsymbol{\Lambda} \cdot \nabla \times \boldsymbol{\Lambda} + \varepsilon \boldsymbol{\Lambda} \cdot \nabla \times \boldsymbol{\lambda} \quad (6.7)$$

and

$$\boldsymbol{\lambda} = c\boldsymbol{\Lambda} + \Lambda^{-2} \boldsymbol{\Lambda} \times (\nabla a + \nabla \times \boldsymbol{\Lambda} - \varepsilon \nabla \times \boldsymbol{\lambda}), \quad (6.8)$$

where $c(\mathbf{r})$ is another scalar field which obeys

$$\boldsymbol{\Lambda} \cdot \nabla c = -\nabla \cdot [\Lambda^{-2} \boldsymbol{\Lambda} \times (\nabla a + \nabla \times \boldsymbol{\Lambda} - \varepsilon \nabla \times \boldsymbol{\lambda})], \quad (6.9)$$

from requiring that $\nabla \cdot \boldsymbol{\lambda} = 0$. Everything is exact up to this point but we note that this representation will generally break down at isolated points where $\boldsymbol{\Lambda} = 0$.

Now we approximate: first consider an ‘outer’ region, well away from the dissipative, cigar-like structures that lie on the separatrices joining stagnation points. We neglect diffusion in the outer region, the fields having a greater length-scale. The leading order outer problem is obtained by simply setting $\varepsilon = 0$ in the above equations (6.7–6.9), leaving a pair of quasi-linear equations for a and c giving transport along characteristics of $\boldsymbol{\Lambda}$, namely

$$\boldsymbol{\Lambda} \cdot \nabla a = -\boldsymbol{\Lambda} \cdot \nabla \times \boldsymbol{\Lambda}, \quad (6.10)$$

$$\boldsymbol{\Lambda} \cdot \nabla c = -\nabla \cdot [\Lambda^{-2} \boldsymbol{\Lambda} \times (\nabla a + \nabla \times \boldsymbol{\Lambda})], \quad (6.11)$$

together with an equation that then reconstructs $\boldsymbol{\lambda}$, from (6.8), which we write as a sum of three terms,

$$\boldsymbol{\lambda} = \boldsymbol{\lambda}_c + \boldsymbol{\lambda}_a + \boldsymbol{\lambda}_\Lambda, \quad (6.12)$$

with

$$\boldsymbol{\lambda}_c = c\boldsymbol{\Lambda}, \quad \boldsymbol{\lambda}_a = \Lambda^{-2}\boldsymbol{\Lambda} \times \nabla a, \quad \boldsymbol{\lambda}_\Lambda = \Lambda^{-2}\boldsymbol{\Lambda} \times (\nabla \times \boldsymbol{\Lambda}). \quad (6.13)$$

Finally for this section, we note that in the outer region, $\boldsymbol{\lambda}_c$ can be calculated explicitly in terms of $\boldsymbol{\Lambda}$ and a . Substitution of (6.13) into (6.3), where the diffusive term involving ε is neglected, yields

$$\nabla \times [(\boldsymbol{\Lambda} \cdot \nabla)(c\boldsymbol{\Lambda} + \Lambda^{-2}\boldsymbol{\Lambda} \times (\nabla a + \nabla \times \boldsymbol{\Lambda}))] = \nabla \times \boldsymbol{f}. \quad (6.14)$$

By virtue of (6.11), this equation takes the form

$$\nabla c \times (\boldsymbol{\Lambda} \cdot \nabla)\boldsymbol{\Lambda} + c\nabla \times ((\boldsymbol{\Lambda} \cdot \nabla)\boldsymbol{\Lambda}) = \nabla \times \boldsymbol{F}, \quad (6.15)$$

where

$$\boldsymbol{F} \equiv \boldsymbol{\Lambda} \nabla \cdot [\Lambda^{-2}\boldsymbol{\Lambda} \times (\nabla a + \nabla \times \boldsymbol{\Lambda})] - (\boldsymbol{\Lambda} \cdot \nabla)[\Lambda^{-2}\boldsymbol{\Lambda} \times (\nabla a + \nabla \times \boldsymbol{\Lambda})] + \boldsymbol{f}. \quad (6.16)$$

Scalar multiplication of (6.15) by $(\boldsymbol{\Lambda} \cdot \nabla)\boldsymbol{\Lambda}$ yields

$$c = \frac{(\nabla \times \boldsymbol{F}) \cdot (\boldsymbol{\Lambda} \cdot \nabla)\boldsymbol{\Lambda}}{[\nabla \times (\boldsymbol{\Lambda} \cdot \nabla)\boldsymbol{\Lambda}] \cdot [\boldsymbol{\Lambda} \cdot \nabla)\boldsymbol{\Lambda}]}. \quad (6.17)$$

Thus singularities of c can arise, where the helicity type term involving $(\boldsymbol{\Lambda} \cdot \nabla)\boldsymbol{\Lambda}$ (i.e., the denominator in (6.17)) vanishes.

6.2 Field in the outer region, near the main separatrix

In the outer region, as the main separatrix is approached, it is observed that the field $\boldsymbol{\Lambda}$ is relatively smooth, as seen from the numerical simulations of CG, and also in view of the leading order Laplacian in (6.2), whereas $\boldsymbol{\lambda}$ develops fine scales. Using the formulation in (5.4) we from now on define $s(\zeta)$ and $\Omega(\zeta)$ by

$$\boldsymbol{\Lambda} = (-s'(\zeta)\rho, \Omega(\zeta)\rho, 2s(\zeta)) + O(\rho^2), \quad (6.18)$$

in cylindrical polar coordinates (ρ, θ, ζ) defined in (5.1) and below. Here the functions $2s(\zeta)/\sqrt{3}$ and $2\Omega(\zeta)\sqrt{3}$ defined for $\boldsymbol{\Lambda}$ are shown in figure 4(a,b), but are not known analytically; nonetheless their functional form is similar to that of the Kolmogorov flow (5.5)

To understand the diffusive $O(\varepsilon^{1/2})$ scaling in the cigars and to determine something of the local structure of the fine-scaled $\boldsymbol{\lambda}$ field the following strategy is adopted: solve the equations (6.10) and (6.11) by integrating along characteristics of $\boldsymbol{\Lambda}$ given locally by (6.18) and reconstruct $\boldsymbol{\lambda}$ via (6.13). As

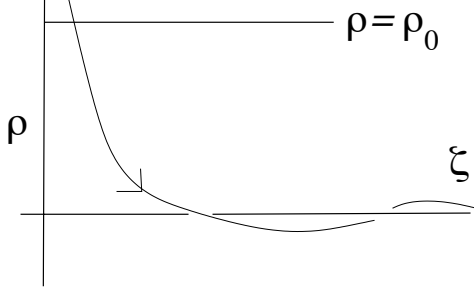


Fig. 5. Schematic figure showing the flow in the (ρ, θ, ζ) coordinates.

the characteristics of $\mathbf{\Lambda}$ approach the origin and are squeezed along the outgoing separatrix, given by $\zeta = O(1)$, $\rho = 0$, high gradients build up and the terms in ε that were earlier neglected increase: when these come into balance with the terms we have retained, we reach the scale at which diffusive effects become important, fixing the width of the dissipative regions.

There are two problems with this approach: first that the incoming values of a and c are determined by the outer solution and links to other cigars: as this is beyond what can be addressed analytically, unknown functions have to be introduced. Secondly, even with the simplified, general local form (6.18), analytical calculations rapidly become unwieldy. The first problem will remain with us, but to ameliorate the second problem we simplify further and consider only the motion near to the origin, in which will simply take the field $\mathbf{\Lambda}$ to be, exactly,

$$\mathbf{\Lambda} = (-\sigma\rho, \omega\rho, 2\sigma\zeta), \quad (6.19)$$

in the local cylindrical polar coordinate system (ρ, ϕ, ζ) . Here σ and ω are taken as constants, which we may identify as

$$\sigma = s'(0), \quad \omega = \Omega(0). \quad (6.20)$$

We also note from (6.19) that

$$\nabla \times \mathbf{\Lambda} = (0, 0, 2\omega), \quad \Lambda^2 = (\omega^2 + \sigma^2)\rho^2 + 4\sigma^2\zeta^2 = 4\sigma^2\zeta^2 + O(\rho^2). \quad (6.21)$$

Our strategy now is to solve the outer, diffusionless equations (6.10–6.11) for transport of a and c for the simplified form (6.19) of $\mathbf{\Lambda}$. This is done exactly, but then to see how large the neglected, diffusion terms are, we approximate by taking $\zeta = O(1)$ but $\rho \ll 1$, so our results are valid in the outer region, near to the origin, on the outward-going separatrix, as depicted schematically in figure 5. Of course, by the time $\zeta = O(1)$ we are, strictly speaking, away from the stagnation point at the origin and the form (6.19) that we are using no longer applies. However the above form is sufficient to obtain the overall structure of the outer solution as the separatrix is approached, together with the scaling of the diffusive layer width.

Equation (6.10) becomes

$$\mathbf{\Lambda} \cdot \nabla a = -4\omega\sigma\zeta, \quad (6.22)$$

and letting t be a time parameter along characteristics, we integrate this in the standard way, with

$$\dot{\rho} = -\sigma\rho, \quad \dot{\theta} = \omega, \quad \dot{\zeta} = 2\sigma\zeta, \quad \dot{a} = -4\omega\sigma\zeta, \quad (6.23)$$

and the solution in terms of initial conditions on a characteristic,

$$\rho = \rho_0 e^{-\sigma t}, \quad \theta = \theta_0 + \omega t, \quad \zeta = \zeta_0 e^{2\sigma t}, \quad a = a_0 + 2\omega\zeta_0(1 - e^{2\sigma t}). \quad (6.24)$$

If we suppose that we specify the incoming values of a on a surface $\rho = \rho_0 > 0$ (see figure 5) with

$$a_0 = a(\rho_0, \theta_0, \zeta_0) = A(\theta_0, \zeta_0) \quad (6.25)$$

at $t = 0$, then we have the solution:

$$a(\rho, \theta, \zeta) = A[\theta + \sigma^{-1}\omega \log(\rho/\rho_0), \zeta\rho^2/\rho_0^2] + 2\omega\zeta(\rho^2/\rho_0^2 - 1). \quad (6.26)$$

Here A gives the form of the field being carried in from the outer region, and we do not know much about it, except that it has 3-fold rotational symmetry (see figure 3 and figure 13 of CG). It is perhaps helpful to think of A as being some function of order unity with the appropriate symmetry, for example $A = A_0 + A_3 \cos 3\theta$.

Given a we can now reconstruct the appropriate part of $\mathbf{\lambda}$ in (6.13). We have

$$\begin{aligned} \nabla a &= (\omega\sigma^{-1}\rho^{-1}A_\theta + 2\zeta\rho\rho_0^{-2}(A_\zeta + 2\omega), \rho^{-1}A_\theta, \rho^2\rho_0^{-2}A_\zeta + 2\omega(\rho^2\rho_0^{-2} - 1)) \\ &= \sigma^{-1}\rho^{-1}(\omega A_\theta, \sigma A_\theta, -2\omega\sigma\rho) + O(\rho), \end{aligned} \quad (6.27)$$

and so

$$\mathbf{\lambda}_a \equiv \Lambda^{-2}\mathbf{\Lambda} \times \nabla a = 2\Lambda^{-2}(-\sigma, \omega, 0)\zeta\rho^{-1}A_\theta + O(\rho^0), \quad (6.28)$$

as $\rho \rightarrow 0$, where A_θ denotes the derivative of A with respect to its first argument. Here we have obtained a component growing as ρ^{-1} which arises because of the incoming values of A on different characteristics being squeezed together.

6.3 The effect of diffusive terms

With this component of $\mathbf{\lambda}$ in hand, we can now revisit the diffusive equation (6.7). We calculate

$$\nabla \times \mathbf{\lambda}_a = 2\Lambda^{-2}(\omega^2 + \sigma^2)(0, 0, \sigma^{-1})\zeta\rho^{-2}A_{\theta\theta} + O(\rho^{-1}), \quad (6.29)$$

and

$$\mathbf{\Lambda} \cdot \nabla \times \mathbf{\lambda}_a = 4\Lambda^{-2}(\omega^2 + \sigma^2)\zeta^2\rho^{-2}A_{\theta\theta} + O(\rho^{-1}). \quad (6.30)$$

This now has a ρ^{-2} growth, by virtue of differentiating A again. In equation (6.7) it is clear that the final $\varepsilon \mathbf{\Lambda} \cdot \nabla \times \mathbf{\lambda}_a$ term with diffusion will be the same order as the term $\mathbf{\Lambda} \cdot \nabla \times \mathbf{\Lambda} = 4\omega\sigma\zeta$ we originally included, when $\varepsilon\rho^{-2} = O(1)$. This gives the $\rho = O(\sqrt{\varepsilon})$ scaling of the diffusive cigar width. Similarly at these values of r , in (6.8) and (6.9) the terms $\varepsilon \nabla \times \mathbf{\lambda}_a$ become of similar magnitude to $\nabla \times \mathbf{\Lambda}$ (though note here that the ∇a terms are actually larger in magnitude at this point).

This is the main part of the argument: although we have simplified by focusing solely on $\mathbf{\lambda}_a$ in (6.13), consideration of the scalar c and component $\mathbf{\lambda}_c$ does not affect the discussion, nor does $\mathbf{\lambda}_{\mathbf{\Lambda}}$, given straightforwardly by

$$\mathbf{\lambda}_{\mathbf{\Lambda}} \equiv \Lambda^{-2} \mathbf{\Lambda} \times (\nabla \times \mathbf{\Lambda}) = 2\Lambda^{-2} \omega(\omega, \sigma, 0) \rho, \quad (6.31)$$

and so is negligible. To check this we now look at the $\varepsilon = 0$ equation (6.11) for c and the corresponding component $\mathbf{\lambda}_c$. After a straightforward calculation (6.11) becomes

$$\mathbf{\Lambda} \cdot \nabla c = -12\Lambda^{-4} \sigma(\omega^2 + \sigma^2) \zeta A_{\theta} + O(\rho). \quad (6.32)$$

The key point is that the right-hand side is of order unity as $\rho \rightarrow 0$, as was the case for a in (6.22). Thus without solving the equation in detail, it is clear that the solution analogous to (6.26) for a will take the form

$$c(\rho, \theta, \zeta) = C[\theta + \omega\sigma^{-1} \log(\rho/\rho_0), \zeta\rho^2/\rho_0^2] + C_{\text{PI}}(\rho, \theta, \zeta), \quad (6.33)$$

where $C(\theta_0, \zeta_0)$ gives the incoming values of c on the surface $\rho = \rho_0$, as before and the particular integral C_{PI} involves A but is of order unity as $\rho \rightarrow 0$.

Now when we reconstruct $\mathbf{\lambda}$ via (6.13), the component $c\mathbf{\Lambda} = O(1)$ along streamlines will be subdominant to the component $\mathbf{\Lambda} \times \nabla a = O(\rho^{-1})$, the inverse power of ρ arising from taking the gradient. Thus our focus on $\mathbf{\lambda}_a$ in the above discussion of the diffusive breakdown of the outer solution is justified and we have

$$\mathbf{\lambda} = \mathbf{\lambda}_a + O(1) = 2\Lambda^{-2}(-\sigma, \omega, 0) \zeta \rho^{-1} A_{\theta} + O(1), \quad (6.34)$$

as $\rho \rightarrow 0$ on the outgoing separatrix. As a by-product of our calculations we observe that the small-scale field $\mathbf{\lambda}$ will show components $\mathbf{\lambda}_a$ perpendicular to streamlines that diverge as ρ^{-1} as the separatrix is approached from the outer solution. These will peak at levels $\mathbf{\lambda} = O(\varepsilon^{-1/2})$ when diffusive suppression begins to occur at scales $\rho = \sqrt{\varepsilon}$. This is in keeping with the scalings seen by CG, who note that $\mathbf{\Lambda}_{-} = \varepsilon \mathbf{\lambda} = O(\sqrt{\varepsilon})$ near the separatrices (their section 3.2.1, figures 13 and 16). In view of the $\cos 3\theta$ dependence of the leading field identified here, this component must go to zero on the axis itself and is presumably strongly suppressed by diffusion. Thus we cannot make a detailed link with figure 4: the field here originates with the mean component of A ,

independent of θ , for which the onset of diffusion will be delayed until smaller values of ρ . This also presumably explains the structure seen in figure 3 (most clearly in (b)) or figure 13 of CG, with three incoming sheets of field merging in an axisymmetric ‘collar’ at smaller values of ρ . In this way, there could be several nested boundary layers along the separatrices in the limit $\varepsilon \rightarrow 0$.

7 Existence of weak steady-state solutions

We consider now the system of equations (6.2) and (6.3) in Elsasser variables, together with the solenoidality conditions

$$\nabla \cdot \boldsymbol{\lambda} = \nabla \cdot \boldsymbol{\Lambda} = 0. \quad (7.1)$$

In this section we define weak solutions to these equations and formally prove their existence, adapting the approach of Ladyzhenskaya (1969). In the next two sections we will show that the weak solutions are classical smooth functions, satisfying the equations at any point in space.

We start by recalling some definitions. Consider the class of functions whose domain is the periodicity cell $\mathbb{T}^3 \equiv [0, 2\pi]^3$. The norm in the Lebesgue space $L_p(\mathbb{T}^3)$ is defined, for $p \geq 1$, as

$$\|\boldsymbol{\Phi}\|_p \equiv \left(\int_{\mathbb{T}^3} |\boldsymbol{\Phi}|^p dV \right)^{1/p}. \quad (7.2)$$

Since in the above-mentioned class $\mathcal{I} - \nabla^2$ is a positively defined self-adjoint operator (where \mathcal{I} is the identity), whose eigenfunctions are Fourier harmonics, we can define in the usual way the powers $(\mathcal{I} - \nabla^2)^\alpha$ for an arbitrary real α , by considering Fourier series. For $\mathbf{r} \in \mathbb{R}^3$ and any

$$\boldsymbol{\Phi} = \sum_{\mathbf{n} \neq 0} \boldsymbol{\Phi}_{\mathbf{n}} e^{i\mathbf{n} \cdot \mathbf{r}}, \quad (7.3)$$

$$(\mathcal{I} - \nabla^2)^\alpha \boldsymbol{\Phi} \equiv \sum_{\mathbf{n} \neq 0} (1 + |\mathbf{n}|^2)^\alpha \boldsymbol{\Phi}_{\mathbf{n}} e^{i\mathbf{n} \cdot \mathbf{r}}. \quad (7.4)$$

The Sobolev space $W_p^s(\mathbb{T}^3)$ is defined for $p \geq 1$, as the closure in the norm

$$\|\boldsymbol{\Phi}\|_{s,p} \equiv \|(\mathcal{I} - \nabla^2)^{s/2} \boldsymbol{\Phi}\|_p \quad (7.5)$$

of the set of infinitely smooth periodic functions, whose domain is \mathbb{T}^3 . (Evidently, $L_p(\mathbb{T}^3) = W_p^0(\mathbb{T}^3)$.) We will work in the subspace of zero-mean vector fields, in which the operator $-\nabla^2$ can be used instead of $\mathcal{I} - \nabla^2$ in these definitions. In particular, we define (without introducing a new notation) a norm, equivalent to (7.5), in the subspace of zero-mean fields in $W_p^s(\mathbb{T}^3)$ as

$$\|\boldsymbol{\Phi}\|_{s,p} \equiv \|(-\nabla^2)^{s/2} \boldsymbol{\Phi}\|_p. \quad (7.6)$$

Since the Laplacian is a self-adjoint operator, in the important particular case $p = 2$ this implies

$$\|\Phi\|_{s,2}^2 = \int_{\mathbb{T}^3} \Phi \cdot (-\nabla^2)^s \Phi \, dV. \quad (7.7)$$

We will employ the following:

Embedding theorem (see Bergh & Löfström (1976), Taylor (1981) and references therein).

(i) For $s > N/p$, $W_p^s(\mathbb{T}^3) \subset C(\mathbb{T}^3)$.

(ii) For $0 < s < N/p$ and $q = Np/(N - ps)$, $W_p^s(\mathbb{T}^3) \subset L_q(\mathbb{T}^3)$ (in particular, $\|\Phi\|_q \leq C_{s,p} \|\Phi\|_{s,p}$).

Consider then, the set of infinitely smooth solenoidal zero-mean periodic functions, whose domain is the periodicity cell $\mathbb{T}^3 \equiv [0, 2\pi]^3$, and denote by \mathcal{H} its closure in the Sobolev space $W_2^1(\mathbb{T}^3)$. A pair of vector fields $\Lambda \in \mathcal{H}$, $\lambda \in \mathcal{H}$ is a *weak solution* to the system (6.2), (6.3) and (7.1), if the integral identities

$$\int_{\mathbb{T}^3} \left(\sum_{k=1}^3 \frac{\partial \Lambda}{\partial x_k} \cdot \frac{\partial \Phi}{\partial x_k} + ((\lambda \cdot \nabla) \Lambda - f) \cdot \Phi \right) dV = 0 \quad (7.8)$$

and

$$\int_{\mathbb{T}^3} \left(\varepsilon \sum_{k=1}^3 \frac{\partial \lambda}{\partial x_k} \cdot \frac{\partial \Phi}{\partial x_k} + ((\Lambda \cdot \nabla) \lambda - f) \cdot \Phi \right) dV = 0 \quad (7.9)$$

hold true for any vector field $\Phi \in \mathcal{H}$. (If Λ and λ are smooth, these identities immediately follow from (6.2) and (6.3).) By Hölder's inequality and the embedding theorem, for any function $f \in W_2^1(\mathbb{T}^3)$,

$$\|f\|_4 \leq \|f\|_2^{1/4} \|f\|_6^{3/4} \leq C_1 \|f\|_2^{1/4} \|f\|_{1,2}^{3/4} \leq C_1 \|f\|_{1,2}, \quad (7.10)$$

where C_1 is a constant independent of f . Consequently, the Cauchy–Bunyakovsky–Schwarz inequality implies that the integrals involving nonlinear terms admit the bounds

$$\begin{aligned} \left| \int_{\mathbb{T}^3} ((\lambda \cdot \nabla) \Lambda) \cdot \Phi \, dV \right| &= \left| \int_{\mathbb{T}^3} \sum_{k=1}^3 \lambda_k \Lambda \cdot \frac{\partial \Phi}{\partial x_k} \, dV \right| \\ &\leq \sum_{j=1}^3 \sum_{k=1}^3 \|\lambda_k\|_4 \|\Lambda_j\|_4 \left\| \frac{\partial \Phi_j}{\partial x_k} \right\|_2 \leq C_2 \|\lambda\|_{1,2} \|\Lambda\|_{1,2} \|\Phi\|_{1,2}, \end{aligned} \quad (7.11)$$

C_2 being a constant independent of λ, Λ and Φ , and similarly

$$\left| \int_{\mathbb{T}^3} ((\Lambda \cdot \nabla) \lambda) \cdot \Phi \, dV \right| \leq C_2 \|\lambda\|_{1,2} \|\Lambda\|_{1,2} \|\Phi\|_{1,2}. \quad (7.12)$$

Thus the integrals are well-defined.

Consider the scalar product in \mathcal{H}

$$[\Phi_1, \Phi_2] \equiv \int_{\mathbb{T}^3} \sum_{k=1}^3 \frac{\partial \Phi_1}{\partial x_k} \cdot \frac{\partial \Phi_2}{\partial x_k} dV. \quad (7.13)$$

Integrating by parts we express the identities (7.8) and (7.9) in an alternative form,

$$[\Lambda - \mathcal{A}(\lambda, \Lambda) - \tilde{f}, \Phi] = 0, \quad (7.14)$$

and

$$[\varepsilon \lambda - \mathcal{A}(\Lambda, \lambda) - \tilde{f}, \Phi] = 0. \quad (7.15)$$

Here

$$\tilde{f} = -(\nabla^2)^{-1} f, \quad (7.16)$$

$(\nabla^2)^{-1}$ denoting, as usual, the inverse Laplacian, and

$$\mathcal{A}(\lambda, \Lambda) \equiv (\nabla^2)^{-1} \mathcal{P}((\lambda \cdot \nabla) \Lambda) \quad (7.17)$$

is a bilinear operator, where \mathcal{P} is the projection onto the subspace of solenoidal vector fields. (In fact, for the Kolmogorov forcing $\tilde{f} = f$, but in what follows we do not employ this equality.)

Using (7.7) for $s = 1$, we find

$$\begin{aligned} \|\mathcal{A}(\lambda, \Lambda)\|_{1,2}^2 &= - \int_{\mathbb{T}^3} \mathcal{P}((\lambda \cdot \nabla) \Lambda) \cdot (\nabla^2)^{-1} \mathcal{P}((\lambda \cdot \nabla) \Lambda) dV \\ &= \sum_{j=1}^3 \sum_{k=1}^3 \int_{\mathbb{T}^3} \lambda_k \Lambda \cdot (\nabla^2)^{-1} \mathcal{P} \left[\frac{\partial^2}{\partial x_j \partial x_k} (\lambda_j \Lambda) \right] dV. \end{aligned} \quad (7.18)$$

For any

$$\Phi = \sum_{n \neq 0} \Phi_n e^{in \cdot r}, \quad (7.19)$$

$$(\nabla^2)^{-1} \mathcal{P} \left[\frac{\partial^2}{\partial x_j \partial x_k} \Phi \right] = \sum_{n \neq 0} \left(\Phi_n - \frac{\Phi_n \cdot n}{|n|^2} \right) \frac{n_j n_k}{|n|^2} e^{in \cdot r}, \quad (7.20)$$

and therefore

$$\left\| (\nabla^2)^{-1} \mathcal{P} \left[\frac{\partial^2}{\partial x_j \partial x_k} \Phi \right] \right\|_2 \leq \|\Phi\|_2. \quad (7.21)$$

Now we develop (7.18), using Hölder's inequality and the embedding theorem,

$$\|\mathcal{A}(\lambda, \Lambda)\|_{1,2}^2 \leq \sum_{j=1}^3 \sum_{k=1}^3 \sum_{l=1}^3 \|\lambda_k\|_4 \|\Lambda_l\|_4 \|\lambda_j \Lambda\|_2 \leq C_3 \|\lambda\|_{1,2}^2 \|\Lambda\|_{1,2}^2, \quad (7.22)$$

which shows that $\mathcal{A} : \mathcal{H} \otimes \mathcal{H} \rightarrow \mathcal{H}$.

Thus, we have shown that for $\Lambda \in \mathcal{H}$ and $\lambda \in \mathcal{H}$ the first factors in the scalar products in the right-hand sides of (7.14) and (7.15) belong to \mathcal{H} . Since

smooth vector fields are dense in \mathcal{H} in the norm induced by the scalar product $[\cdot, \cdot]$, (7.14) and (7.15) are equivalent to equations

$$\Lambda - \mathcal{A}(\boldsymbol{\lambda}, \Lambda) - \tilde{\mathbf{f}} = \mathbf{0} \quad (7.23)$$

and

$$\boldsymbol{\lambda} - \varepsilon^{-1}(\mathcal{A}(\Lambda, \boldsymbol{\lambda}) + \tilde{\mathbf{f}}) = \mathbf{0}, \quad (7.24)$$

respectively, understood as equalities in \mathcal{H} .

The existence of solutions to the system (7.23), (7.24) is guaranteed by the Leray–Schauder principle (see Leray & Schauder (1934) and Ladyzhenskaya (1969)) under two conditions:

(i) The operator $\mathcal{B} : \mathcal{H} \otimes \mathcal{H} \rightarrow \mathcal{H} \otimes \mathcal{H}$ defined as

$$\mathcal{B}(\Lambda, \boldsymbol{\lambda}) = (\mathcal{A}(\boldsymbol{\lambda}, \Lambda), \mathcal{A}(\Lambda, \boldsymbol{\lambda})/\varepsilon) \quad (7.25)$$

is compact, i.e. $\mathcal{B}(\Lambda_n, \boldsymbol{\lambda}_n)$ is a strongly converging sequence in $\mathcal{H} \otimes \mathcal{H}$ for any sequence $(\Lambda_n, \boldsymbol{\lambda}_n)$ weakly converging in $\mathcal{H} \otimes \mathcal{H}$.

(ii) Any solution to the set of equations

$$\Lambda - \mu(\mathcal{A}(\boldsymbol{\lambda}, \Lambda) + \tilde{\mathbf{f}}) = 0, \quad \boldsymbol{\lambda} - \mu\varepsilon^{-1}(\mathcal{A}(\Lambda, \boldsymbol{\lambda}) + \tilde{\mathbf{f}}) = 0 \quad (7.26)$$

belongs to a ball in $\mathcal{H} \otimes \mathcal{H}$ of a radius independent of μ for $0 \leq \mu \leq 1$.

The proof of (i) relies on the embedding theorem for Sobolev spaces, whereby the embedding $W_2^1(\mathbb{T}^3) \rightarrow L_q(\mathbb{T}^3)$ is compact for $q < 6$, i.e., $\|\boldsymbol{\lambda}^n - \boldsymbol{\lambda}^m\|_q + \|\Lambda^n - \Lambda^m\|_q \rightarrow 0$ for $m, n \rightarrow \infty$, for any sequence $(\boldsymbol{\lambda}^n, \Lambda^n)$ weakly converging in $W_2^1(\mathbb{T}^3) \otimes W_2^1(\mathbb{T}^3)$. It is enough to prove that $\mathcal{A}(\boldsymbol{\lambda}^n, \Lambda^n)$ converges strongly in \mathcal{H} . For any $\Phi \in \mathcal{H}$,

$$[\mathcal{A}(\boldsymbol{\lambda}^n, \Lambda^n) - \mathcal{A}(\boldsymbol{\lambda}^m, \Lambda^m), \Phi] = \int_{\mathbb{T}^3} \sum_{k=1}^3 (\lambda_k^n \Lambda^n - \lambda_k^m \Lambda^m) \cdot \frac{\partial \Phi}{\partial x_k} dV \quad (7.27)$$

$$= \int_{\mathbb{T}^3} \sum_{k=1}^3 \lambda_k^n (\Lambda^n - \Lambda^m) \cdot \frac{\partial \Phi}{\partial x_k} dV + \int_{\mathbb{T}^3} \sum_{k=1}^3 (\lambda_k^n - \lambda_k^m) \Lambda^m \cdot \frac{\partial \Phi}{\partial x_k} dV. \quad (7.28)$$

Hence, by the same arguments as were used to derive (7.11), we obtain

$$\|[\mathcal{A}(\boldsymbol{\lambda}^n, \Lambda^n) - \mathcal{A}(\boldsymbol{\lambda}^m, \Lambda^m), \Phi]\|_{1,2} \leq C_4(\|\boldsymbol{\lambda}^n\|_{1,2}\|\Lambda^n - \Lambda^m\|_4 + \|\boldsymbol{\lambda}^n - \boldsymbol{\lambda}^m\|_4\|\Lambda^m\|_{1,2})\|\Phi\|_{1,2}. \quad (7.29)$$

Here $\Phi \in \mathcal{H}$ is arbitrary; letting $\Phi = \mathcal{A}(\boldsymbol{\lambda}^n, \Lambda^n) - \mathcal{A}(\boldsymbol{\lambda}^m, \Lambda^m)$, from this inequality we deduce

$$\|\mathcal{A}(\boldsymbol{\lambda}^n, \Lambda^n) - \mathcal{A}(\boldsymbol{\lambda}^m, \Lambda^m)\|_{1,2} \leq C_5(\|\Lambda^n - \Lambda^m\|_4 + \|\boldsymbol{\lambda}^n - \boldsymbol{\lambda}^m\|_4), \quad (7.30)$$

where the constant C_5 is independent of m and n , since weak convergence of $(\boldsymbol{\lambda}^n, \boldsymbol{\Lambda}^n)$ in $W_2^1(\mathbb{T}^3) \otimes W_2^1(\mathbb{T}^3)$ implies the uniform boundedness of $\|\boldsymbol{\lambda}^n\|_{1,2}$ and $\|\boldsymbol{\Lambda}^n\|_{1,2}$. Thus we have established that $\|\mathcal{A}(\boldsymbol{\lambda}^n, \boldsymbol{\Lambda}^n) - \mathcal{A}(\boldsymbol{\lambda}^m, \boldsymbol{\Lambda}^m)\|_{1,2} \rightarrow 0$ for $m, n \rightarrow \infty$, as desired.

To prove (ii), we consider the problem (7.26) in the form of integral equations, analogous to (7.8) and (7.9),

$$\int_{\mathbb{T}^3} \left(\sum_{k=1}^3 \frac{\partial \boldsymbol{\Lambda}}{\partial x_k} \cdot \frac{\partial \boldsymbol{\Phi}}{\partial x_k} + \mu((\boldsymbol{\lambda} \cdot \nabla) \boldsymbol{\Lambda} - \boldsymbol{f}) \cdot \boldsymbol{\Phi} \right) dV = 0, \quad (7.31)$$

$$\int_{\mathbb{T}^3} \left(\sum_{k=1}^3 \frac{\partial \boldsymbol{\lambda}}{\partial x_k} \cdot \frac{\partial \boldsymbol{\Phi}}{\partial x_k} + \frac{\mu}{\varepsilon}((\boldsymbol{\Lambda} \cdot \nabla) \boldsymbol{\lambda} - \boldsymbol{f}) \cdot \boldsymbol{\Phi} \right) dV = 0, \quad (7.32)$$

which are satisfied for any $\boldsymbol{\Phi} \in \mathcal{H}$. Let $\boldsymbol{\Phi} = \boldsymbol{\Lambda}$ in (7.31) and $\boldsymbol{\Phi} = \boldsymbol{\lambda}$ in (7.32). Due to solenoidality of $\boldsymbol{\lambda}$ and $\boldsymbol{\Lambda}$ the nonlinear terms vanish, and we find from the identities (7.31) and (7.32)

$$[\boldsymbol{\Lambda}, \boldsymbol{\Lambda}] = \mu \int_{\mathbb{T}^3} \boldsymbol{f} \cdot \boldsymbol{\Lambda} dV \leq \mu C_6 \|\boldsymbol{\Lambda}\|_2 \|\boldsymbol{f}\|_2, \quad \Rightarrow \quad \|\boldsymbol{\Lambda}\|_{1,2} \leq \mu C_7 \|\boldsymbol{f}\|_2, \quad (7.33)$$

$$[\boldsymbol{\lambda}, \boldsymbol{\lambda}] = \mu \varepsilon^{-1} \int_{\mathbb{T}^3} \boldsymbol{f} \cdot \boldsymbol{\lambda} dV \leq \mu \varepsilon^{-1} C_6 \|\boldsymbol{\lambda}\|_2 \|\boldsymbol{f}\|_2, \quad \Rightarrow \quad \|\boldsymbol{\lambda}\|_{1,2} \leq \mu \varepsilon^{-1} C_7 \|\boldsymbol{f}\|_2, \quad (7.34)$$

since the norm, induced by the scalar product $[\cdot, \cdot]$ in \mathcal{H} , is equivalent to the norm (7.7) in $W_2^1(\mathbb{T}^3)$. These inequalities establish the existence of a weak solution $\boldsymbol{\Lambda} \in \mathcal{H}$, $\boldsymbol{\lambda} \in \mathcal{H}$ to the problem (6.2), (6.3) and (7.1), admitting the bounds

$$\|\boldsymbol{\Lambda}\|_{1,2} \leq C_7 \|\boldsymbol{f}\|_2, \quad \|\boldsymbol{\lambda}\|_{1,2} \leq C_7 \varepsilon^{-1} \|\boldsymbol{f}\|_2. \quad (7.35)$$

8 Bounds for weak solutions in $W_2^2(\mathbb{T}^3)$

In this section we obtain bounds for the norms of the solution in the spaces $W_2^{5/4}(\mathbb{T}^3)$ and $W_2^2(\mathbb{T}^3)$.

Consider the Fourier series

$$\boldsymbol{\Lambda} = \sum_{\boldsymbol{n} \neq 0} \boldsymbol{\Lambda}_{\boldsymbol{n}} e^{i\boldsymbol{n} \cdot \boldsymbol{r}}, \quad (8.1)$$

and smooth vector fields

$$\boldsymbol{\Lambda}^M = \sum_{\boldsymbol{n} \neq 0, |\boldsymbol{n}| \leq M} \boldsymbol{\Lambda}_{\boldsymbol{n}} e^{i\boldsymbol{n} \cdot \boldsymbol{r}} \in \mathcal{H}. \quad (8.2)$$

Scalar multiplying in $L_2(\mathbb{T}^3)$ (7.23) by $(-\nabla^2)^{5/4} \boldsymbol{\Lambda}^M \in \mathcal{H}$, using self-adjointness of the Laplacian, solenoidality of $\boldsymbol{\Lambda}$ and hence of $\boldsymbol{\Lambda}^M$, and orthogonality of

potential and solenoidal fields in $L_2(\mathbb{T}^3)$, we obtain

$$\begin{aligned} \int_{\mathbb{T}^3} \mathbf{\Lambda} \cdot (-\nabla^2)^{5/4} \mathbf{\Lambda}^M dV + \int_{\mathbb{T}^3} (\boldsymbol{\lambda} \cdot \nabla) \mathbf{\Lambda} \cdot (-\nabla^2)^{1/4} \mathbf{\Lambda}^M dV \\ = \int_{\mathbb{T}^3} \tilde{\mathbf{f}} \cdot (-\nabla^2)^{5/4} \mathbf{\Lambda}^M dV. \end{aligned} \quad (8.3)$$

Note that

$$\|(-\nabla^2)^{1/4} ((-\nabla^2)^{1/4} \mathbf{\Lambda}^M)\|_2 = \|\mathbf{\Lambda}^M\|_{1,2} \leq \|\mathbf{\Lambda}\|_{1,2}, \quad (8.4)$$

and hence $(-\nabla^2)^{1/4} \mathbf{\Lambda}^M \in W_2^{1/2}$, and by part (ii) of the Theorem

$$\|(-\nabla^2)^{1/4} \mathbf{\Lambda}^M\|_3 \leq C_{1/2,2} \|\mathbf{\Lambda}\|_{1,2}. \quad (8.5)$$

This, together with (7.35), implies a bound for the first integral

$$\begin{aligned} \left| \int_{\mathbb{T}^3} (\boldsymbol{\lambda} \cdot \nabla) \mathbf{\Lambda} \cdot (-\nabla^2)^{1/4} \mathbf{\Lambda}^M dV \right| &\leq \|\boldsymbol{\lambda}\|_6 \|\nabla \mathbf{\Lambda}\|_2 \|(-\nabla^2)^{1/4} \mathbf{\Lambda}^M\|_3, \\ &\leq C_{1/2,2} \|\mathbf{\Lambda}\|_{1,2}^2 \|\boldsymbol{\lambda}\|_{1,2} \leq C_8/\varepsilon. \end{aligned} \quad (8.6)$$

Also,

$$\left| \int_{\mathbb{T}^3} \tilde{\mathbf{f}} \cdot (-\nabla^2)^{5/4} \mathbf{\Lambda}^M dV \right| \leq \|\mathbf{\Lambda}\|_{1,2} \|(-\nabla^2)^{3/4} \tilde{\mathbf{f}}\|_2 \leq C_9, \quad (8.7)$$

and hence we find from the identity (8.3)

$$\|(-\nabla^2)^{5/8} \mathbf{\Lambda}\|_2^2 = \sup_M \int_{\mathbb{T}^3} \mathbf{\Lambda} \cdot (-\nabla^2)^{5/4} \mathbf{\Lambda}^M dV \leq C_{10} \varepsilon^{-1}. \quad (8.8)$$

Similarly, (7.24) yields

$$\|(-\nabla^2)^{5/8} \boldsymbol{\lambda}\|_2^2 \leq C_{10} \varepsilon^{-3}. \quad (8.9)$$

(Here the constant C_{10} is independent of $\varepsilon \leq 1$, but depends on the forcing $\tilde{\mathbf{f}}$.) We have therefore demonstrated that $\boldsymbol{\lambda} \in W_2^{5/4}(\mathbb{T}^3)$ and $\mathbf{\Lambda} \in W_2^{5/4}(\mathbb{T}^3)$.

Consequently, $(-\nabla^2)^{1/2} \mathbf{\Lambda}^M \in W_2^{1/4}(\mathbb{T}^3)$ and $(-\nabla^2)^{1/2} \mathbf{\Lambda}^M \in W_2^{1/4}(\mathbb{T}^3)$. Using part (ii) of the theorem, we find

$$\|\partial \mathbf{\Lambda} / \partial x_k\|_{12/5} \leq C_{1/4,2} \|(-\nabla^2)^{1/8} (\partial \mathbf{\Lambda} / \partial x_k)\|_2 \leq C_{1/4,2} \|(-\nabla^2)^{5/8} \mathbf{\Lambda}\|_2 \quad (8.10)$$

and

$$\|\mathbf{\Lambda}\|_{12} \leq C_{5/4,2} \|(-\nabla^2)^{5/8} \mathbf{\Lambda}\|_2. \quad (8.11)$$

Similarly,

$$\|\partial \boldsymbol{\lambda} / \partial x_k\|_{12/5} \leq C_{1/4,2} \|(-\nabla^2)^{5/8} \boldsymbol{\lambda}\|_2, \quad \|\boldsymbol{\lambda}\|_{12} \leq C_{5/4,2} \|(-\nabla^2)^{5/8} \boldsymbol{\lambda}\|_2. \quad (8.12)$$

Scalar multiplying in $L_2(\mathbb{T}^3)$ (7.23) by $(-\nabla^2)^2 \mathbf{\Lambda}^M$, we obtain

$$\|(-\nabla^2) \mathbf{\Lambda}^M\|_2^2 + \int_{\mathbb{T}^3} (\boldsymbol{\lambda} \cdot \nabla) \mathbf{\Lambda} \cdot (-\nabla^2) \mathbf{\Lambda}^M dV = \int_{\mathbb{T}^3} \tilde{\mathbf{f}} \cdot (-\nabla^2)^2 \mathbf{\Lambda}^M dV. \quad (8.13)$$

By Hölder's inequality,

$$\left| \int_{\mathbb{T}^3} (\boldsymbol{\lambda} \cdot \nabla) \boldsymbol{\Lambda} \cdot (-\nabla^2) \boldsymbol{\Lambda}^M dV \right| \leq \|\boldsymbol{\lambda}\|_{12} \|\nabla \boldsymbol{\Lambda}\|_{12/5} \|(-\nabla^2) \boldsymbol{\Lambda}^M\|_2 \quad (8.14)$$

and hence from (8.13) and (8.10–8.12),

$$\begin{aligned} \|(-\nabla^2) \boldsymbol{\Lambda}^M\|_2^2 &\leq C_{11} \|(-\nabla^2)^{5/8} \boldsymbol{\lambda}\|_2^2 \|(-\nabla^2)^{5/8} \boldsymbol{\Lambda}\|_2^2 \\ &\quad + \frac{1}{2} \|(-\nabla^2) \boldsymbol{\Lambda}^M\|_2^2 + \|\boldsymbol{f}\|_2 \|(-\nabla^2) \boldsymbol{\Lambda}\|_2, \end{aligned} \quad (8.15)$$

whereby

$$\|(-\nabla^2) \boldsymbol{\Lambda}\|_2^2 = \sup_M \|(-\nabla^2) \boldsymbol{\Lambda}^M\|_2^2 \leq C_{12} \varepsilon^{-4}. \quad (8.16)$$

The same operations applied to (7.24) yield

$$\|(-\nabla^2) \boldsymbol{\lambda}\|_2 \leq C_{12} \varepsilon^{-3}. \quad (8.17)$$

Thus we have demonstrated that $\boldsymbol{\lambda}$ and $\boldsymbol{\Lambda}$ belong to $W_2^2(\mathbb{T}^3)$.

9 Smoothness of weak solutions

Steady-state hydrodynamic and MHD problems are drastically different from the evolutionary ones in that one can incrementally establish the smoothness of their solutions together with the derivatives of arbitrary order (provided the forcing \boldsymbol{f} is smooth). In this section we use (7.23) and (7.24) to show by induction, that $\boldsymbol{\lambda}$ and $\boldsymbol{\Lambda}$ are smooth vector fields and therefore constitute a classical solution to the original system of equations.

We assume that $\boldsymbol{\lambda} \in W_2^{2k}(\mathbb{T}^3)$ and $\boldsymbol{\Lambda} \in W_2^{2k}(\mathbb{T}^3)$ (which is equivalent to $\|(-\nabla^2)^k \boldsymbol{\lambda}\|_2 + \|(-\nabla^2)^k \boldsymbol{\Lambda}\|_2 < \infty$) and $\boldsymbol{f} \in W_2^{2k}(\mathbb{T}^3)$ for $k \geq 1$, and show that $\boldsymbol{\lambda} \in W_2^{2k+2}(\mathbb{T}^3)$ and $\boldsymbol{\Lambda} \in W_2^{2k+2}(\mathbb{T}^3)$.

Scalar multiplying in $L_2(\mathbb{T}^3)$ (7.23) by $(-\nabla^2)^{2k+1} \boldsymbol{\Lambda}^M$, using self-adjointness of the Laplacian, solenoidality of $\boldsymbol{\Lambda}^M$ and orthogonality of potential and solenoidal fields in $L_2(\mathbb{T}^3)$, we obtain

$$\begin{aligned} \int_{\mathbb{T}^3} \boldsymbol{\Lambda} \cdot (-\nabla^2)^{2k+1} \boldsymbol{\Lambda}^M dV &+ \sum_{j=1}^3 \int_{\mathbb{T}^3} \left((-\nabla^2)^{k-1} \frac{\partial}{\partial x_j} (\boldsymbol{\lambda} \cdot \nabla) \boldsymbol{\Lambda} \right) \cdot (-\nabla^2)^k \frac{\partial \boldsymbol{\Lambda}^M}{\partial x_j} dV \\ &= \int_{\mathbb{T}^3} (-\nabla^2)^{k-1/2} \boldsymbol{f} \cdot (-\nabla^2)^{k+1/2} \boldsymbol{\Lambda}^M dV, \end{aligned} \quad (9.1)$$

and thus

$$\begin{aligned} \|(-\nabla^2)^{k+1/2} \mathbf{\Lambda}^M\|_2^2 &\leq \left(\sum_{j=1}^3 \left\| (-\nabla^2)^{k-1} \frac{\partial}{\partial x_j} (\boldsymbol{\lambda} \cdot \nabla) \mathbf{\Lambda} \right\|_2 \right. \\ &\quad \left. + \|(-\nabla^2)^{k-1/2} \mathbf{f}\|_2 \right) \|(-\nabla^2)^{k+1/2} \mathbf{\Lambda}^M\|_2 \end{aligned} \quad (9.2)$$

implying

$$\|\mathbf{\Lambda}\|_{2k+1,2} = \sup_M \|(-\nabla^2)^{k+1/2} \mathbf{\Lambda}^M\|_2 \leq \sum_{j=1}^3 \left\| (-\nabla^2)^{k-1} \frac{\partial}{\partial x_j} (\boldsymbol{\lambda} \cdot \nabla) \mathbf{\Lambda} \right\|_2 + \|\mathbf{f}\|_{2k-1,2}. \quad (9.3)$$

We need therefore to check that the norms in the sum at the right-hand side of this inequality are bounded. By part (i) of the Theorem, the assumption $\boldsymbol{\lambda} \in W_2^{2k}(\mathbb{T}^3)$ and $\mathbf{\Lambda} \in W_2^{2k}(\mathbb{T}^3)$ implies that $\boldsymbol{\lambda}$ and $\mathbf{\Lambda}$ and their derivatives of order up to $2k-2$ are continuous (and hence uniformly bounded) vector fields in \mathbb{T}^3 . By the standard formula for derivatives of products,

$$(-\nabla^2)^{k-1} \frac{\partial}{\partial x_j} (\boldsymbol{\lambda} \cdot \nabla) \mathbf{\Lambda} \quad (9.4)$$

is a linear combination of products of derivatives

$$\frac{\partial^{N_1} \lambda_q}{\partial^{n_1^1} x_1 \partial^{n_2^1} x_2 \partial^{n_3^1} x_3} \frac{\partial^{N_2} \mathbf{\Lambda}}{\partial^{n_1^2} x_1 \partial^{n_2^2} x_2 \partial^{n_3^2} x_3}, \quad (9.5)$$

where $N_i = n_1^i + n_2^i + n_3^i$, $0 \leq N_1 \leq 2k-1$, $N_2 = 2k - N_1$. Thus, each of the terms is continuous and bounded, except maybe for those for $N_1 = 0, 1$ or $2k-1$. If $N_1 = 0$, or $N_1 = 1$ or $2k-1$ for $k > 1$, one of the factors is continuous and the second one is known to belong to $L_2(\mathbb{T}^3)$, and hence their contributions to the right-hand side of (9.3) are finite. The remaining possibility is $k = N_1 = N_2 = 1$, but in this case both factors belong to $L_4(\mathbb{T}^3)$ because $\boldsymbol{\lambda} \in W_2^2(\mathbb{T}^3)$ and $\mathbf{\Lambda} \in W_2^2(\mathbb{T}^3)$ by the results of the previous subsection, and again the respective norms are bounded.

We have thus established that $\mathbf{\Lambda} \in W_2^{2k+1}(\mathbb{T}^3)$. By similar arguments from (7.24) we find $\boldsymbol{\lambda} \in W_2^{2k+1}(\mathbb{T}^3)$.

To proceed, we scalar multiply in $L_2(\mathbb{T}^3)$ (7.23) by $(-\nabla^2)^{2k+2} \mathbf{\Lambda}^M$, and obtain

$$\begin{aligned} \int_{\mathbb{T}^3} \mathbf{\Lambda} \cdot (-\nabla^2)^{2k+2} \mathbf{\Lambda}^M dV &+ \int_{\mathbb{T}^3} ((-\nabla^2)^k (\boldsymbol{\lambda} \cdot \nabla) \mathbf{\Lambda}) \cdot (-\nabla^2)^{k+1} \mathbf{\Lambda}^M dV \\ &= \int_{\mathbb{T}^3} (-\nabla^2)^k \mathbf{f} \cdot (-\nabla^2)^{k+1} \mathbf{\Lambda}^M dV, \end{aligned} \quad (9.6)$$

and therefore

$$\|\mathbf{\Lambda}\|_{2k+2,2} = \sup_M \|(-\nabla^2)^{k+1} \mathbf{\Lambda}^M\|_2 \leq \|(-\nabla^2)^k (\boldsymbol{\lambda} \cdot \nabla) \mathbf{\Lambda}\|_2 + \|\mathbf{f}\|_{2k,2}. \quad (9.7)$$

Since $\mathbf{\Lambda} \in W_2^{2k+1}(\mathbb{T}^3)$ and $\boldsymbol{\lambda} \in W_2^{2k+1}(\mathbb{T}^3)$, by part (i) of the Theorem any derivative of $\mathbf{\Lambda}$ and $\boldsymbol{\lambda}$ of order up to $2k-1$ is continuous in \mathbb{T}^3 . Hence, in the expansion of $(\boldsymbol{\lambda} \cdot \nabla) \mathbf{\Lambda}$ in a linear combination of products (9.5) each term is either continuous, or a product of a continuous function by a function from $L_2(\mathbb{T}^3)$. Thus, (9.7) demonstrates that $\mathbf{\Lambda} \in W_2^{2k+2}(\mathbb{T}^3)$. Similarly (7.24) yields $\boldsymbol{\lambda} \in W_2^{2k+2}(\mathbb{T}^3)$, concluding the demonstration.

Thus mathematical analysis of the problem yields both good and bad news. The good news is that the problem (6.2), (6.3) and (7.1) necessarily has at least one classical solution, meaning in our case infinitely differentiable at each point. Nothing is known about the number of solutions apart from that it is positive, nor is stability of any of the MHD steady states guaranteed. The bad news is that the bounds for the solutions and their derivatives rapidly degrade as $\varepsilon \rightarrow 0$. In particular, the inequalities that we have derived are insufficient to claim that $\varepsilon \nabla^2 \boldsymbol{\lambda} \rightarrow 0$: the relevant L_2 bound we have derived is (8.17).

It is interesting to compare this general result, that is for a general forcing, with our numerical study of dissipative regions in the Archontis case. For example, in section 6.3 we find peak values $\boldsymbol{\lambda} = O(\varepsilon^{-1/2})$ on scales of order $\varepsilon^{1/2}$ indicating the scaling $\varepsilon \nabla^2 \boldsymbol{\lambda} = O(\varepsilon^{-1/2})$. Note that these anomalously high values are concentrated only in cylindrical cigars about the separatrices, of radius $O(\varepsilon^{1/2})$ and so occupy an $O(\varepsilon)$ volume of space. This results in the estimate $\|\boldsymbol{\lambda}\|_{2,2} = O(\varepsilon^{-1})$, which is a significantly milder singularity than the one suggested by our bound (8.17). The high values have a negligible impact on the energy spectrum, there being no peak visible at small scales. This can probably explain the gap between the ‘worst case scenario’ predicted by the rigorous mathematical analysis of the problem and the numerical results: the Sobolev norms, that we have used, prove inefficient in controlling formation of singularities in localised regions, because they are of inherently integral nature. We should also note that our simulations would not be able to resolve structure on scales much smaller than $O(\varepsilon^{1/2})$.

The apparent deterioration of the derivatives of the solution with their order can be a spurious artefact due to imperfection of the proof, or a real attribute of the solutions. It is likely that for some forcing in (6.2) and (6.3) the worst case scenario suggested by these bounds is indeed realised: they are based on the norm bounds provided by the embedding theorem, which are sharp. In any case, this indicates that any naive approach to the study of the limit $\varepsilon \rightarrow 0$ (for a general forcing) whereby the diffusive term in (6.3) is just discarded, is likely to be erroneous; this can only be done in the region outside dissipative structures. In the absence of the dominant elliptic operator, the equations

obtained in this way are not in general guaranteed to have solutions. When they exist, the solutions are likely to develop singularities at some points or on certain manifolds, or possibly on sets of a more complex structure. Note that locally the existence of solutions is not a problem: the difficulty is in gluing together patches of such solutions. The fast dynamo problem embodies a similar difficulty, with small scales of magnetic field occurring in $O(1)$ volumes of space, though with the fields concentrating on multifractal sets (Childress & Gilbert, 1995). Note however, that the $L_2(\mathbb{T}^3)$ norm of $\mathbf{\Lambda}$ is uniformly (over ε) bounded, so the singularities are likely to be more pronounced in the derivatives of the solution, rather than in the solution itself.

10 Discussion

We have presented investigations into the structure of the magnetic field and flow in the equilibrated regime of the Archontis dynamo. Because of the highly three-dimensional nature of the system, application of the available analytical tools yields only rough results of limited value, and we lack any kind of complete solution. What we have done is first to extend the range of diffusivities ε over which the saturation mechanism operates to give the steady state with nearly aligned fields. We have also classified the symmetries of these flows and measured the field structure on the separatrices, home of the cigar-like dissipative regions.

Then, using basic analytical tools, we have investigated the scaling of diffusive terms near the separatrices. Here at leading order the field $\mathbf{\lambda} = \varepsilon^{-1}\mathbf{\Lambda}_-$ that enters from the body of the flow is transported along characteristics of $\mathbf{\Lambda} = \mathbf{\Lambda}_+$. Where these characteristics come together in the compressive flow at the stagnation points, where trajectories spiral in, large gradients in $\mathbf{\lambda}$ are generated, and diffusive terms enter the problem on scales of $\varepsilon^{1/2}$ as found by CG. In more general flows we may expect a similar behaviour, with regions of heightened dissipation localised at points where $\mathbf{\Lambda} = 0$ and along the unstable manifolds of such points. Of course in the Archontis example the unstable manifolds link the stagnation points and so the topology here is very simple and the dissipative regions very small, of order $O(\varepsilon)$ in volume: in other cases they may wander through the three-dimensional space, giving a picture of much greater complexity, as could be occurring in examples in Cameron & Galloway (2006b). Again wider regions of dissipation, perhaps dense in the space, could occur if examples exist where $\mathbf{\Lambda}$ has no stagnation points; unfortunately the form of $\mathbf{\Lambda}$ is not under our control except where strongly constrained by symmetries. In order to cope with unknown levels of geometrical complexity, an approach based on functional analysis is appropriate, and this is the final part of the paper, in which the existence and smoothness properties of steady solutions are established.

An analogy of the naively truncated equations (namely (6.2, 6.3) with $\varepsilon = 0$) with the Euler equation, which is the subject of intense research, is instructive. A method for the investigation of the evolutionary Euler and Navier–Stokes equations consists of the introduction into the equations of new regularising terms, such as $\varepsilon(-\nabla^2)^\alpha \mathbf{u}$ or $\varepsilon(-\nabla^2)^\beta (\partial \mathbf{u} / \partial t)$. It is known for decades that for $\alpha > 5/4$ solutions to the regularised equations are infinitely differentiable at any $t > 0$; for $\beta \geq 1/2$ and $\beta > 5/6$ one can prove analyticity, at any $t > 0$, of solutions to the Navier–Stokes and Euler equations, respectively (Zheligovsky, 2010). For any α or β below the respective thresholds, the problem is as difficult as the one for the original equation. When the limit $\varepsilon \rightarrow 0$ is considered, the results are so far inconclusive. One can only show that there exist sequences $\varepsilon_k \rightarrow 0$ such that solutions for these ε_k converge to a weak solution to the non-regularised equation, and either the limit weak solution is unique for all such sequences, or there exists a continuum of weak solutions. Whether for $\varepsilon \rightarrow 0$ singularities develop in derivatives of the regularised solutions, and how strong they are if they develop, remains unknown.

The difficulties arise in the general theory, because the bounds for solutions are singular in ε as $\varepsilon \rightarrow 0$. Here the analogy with the Archontis dynamo problem crystallises: in the Archontis problem the diffusive terms can be regarded as a regularisation of the naively truncated diffusionless problem, and we need to find out what happens when the regularisation parameter ε tends to zero. (In the diffusionless, i.e. non-regularised, case it is unclear whether weak steady solutions exist.) We note that the analogy may work both ways: the asymptotic analysis near the separatrix in the Archontis dynamo (which we present in sections 5 and 6) may contain clues to what happens in solutions to the regularised Euler (or even Navier–Stokes) equations in the limit $\varepsilon \rightarrow 0$. Unfortunately, the clues are well hidden, because the regularising term in the Archontis problem is of a different structure, and a very specific symmetric steady solution to the general system of MHD equations is considered.

Besides further attempts to carry out an asymptotic analysis of equations (6.2) and (6.3) and their evolutionary versions, a number of other directions could be pursued in the future, for example investigating time-dependent modifications to the steady Kolmogorov forcing used here, or studying the evolution of superposed large-scale fields and corresponding non-helical transport effects, as in the recent work of Sur & Brandenburg (2009).

Acknowledgements

We are grateful for funding from the Royal Society/CNRS to enable collaboration between ADG and YP, and for a Royal Society visitor grant that supported the work of VZ at the University of Exeter. ADG also thanks the

Leverhulme Trust for their award of a Research Fellowship, during which some of this research was undertaken. VZ was also financed by the grants ANR-07-BLAN-0235 OTARIE from Agence nationale de la recherche, France, and 07-01-92217-CNRSLa from the Russian foundation for basic research. YP thanks A. Miniussi for computing design assistance. Computer time was provided by GENCI (x2010021357) and the Mesocentre SIGAMM machine, hosted by the Observatoire de la Côte d’Azur.

We are grateful to Robert Cameron, David Galloway and Andrew Soward for discussions and comments, particularly during the valuable Isaac Newton Institute (Cambridge, U.K.) programme on Magnetohydrodynamics of Stellar Interiors in 2004. Finally we thank the authors of the open source computer package VAPOR; see www.vapor.ucar.edu.

References

- Archontis, V. 2000 *Study of generation and evolution of magnetic fields in stars using 3D MHD simulations of turbulent flows*. PhD Thesis, Copenhagen University.
- Archontis, V., Dorch, S.B.F. & Nordlund, A. 2007 Nonlinear MHD dynamo operating at equipartition. *Astron. & Astrophys.* **472** 715–726.
- Arnold, V.I. & Korkina, E.I. 1983 The growth of a magnetic field in a three-dimensional steady incompressible flow. *Vest. Mosk. Un. Ta. Ser. 1, Matem. Mekh.*, no. 3, 43–46.
- Bergh, J. & Löfström, J. 1976 *Interpolation spaces*. Springer-Verlag.
- Cameron, R. & Galloway, D. 2006a Saturation properties of the Archontis dynamo. *M. Not. R. Astr. Soc.* **365** 735–746. Referred to as CG in the text.
- Cameron, R. & Galloway, D. 2006b High field strength modified ABC and rotor dynamos. *M. Not. R. Astr. Soc.* **367** 1163–1169.
- Cattaneo, F., Hughes, D.W. & Kim, E.-J. 1996 Suppression of chaos in a simplified dynamo model. *Phys. Rev. Lett.* **76**, 2057–2060.
- Childress, S. & Gilbert, A.D. 1995 *Stretch, twist, fold: the fast dynamo*. Springer-Verlag.
- Childress, S., Kerswell, R.R. & Gilbert, A.D. 2001 Bounds on dissipation for Navier–Stokes flow with Kolmogorov forcing. *Physica D*, **158**, 105–128.
- Courvoisier, A., Hughes, D.W. & Proctor, M.R.E 2010 Self-consistent mean-field magnetohydrodynamics *Proc. R. Soc. A* **466**, 583–601.
- Dobrowolny, M., Mangeney, A. & Veltri, P. 1980 Fully developed anisotropic hydromagnetic turbulence in interplanetary space. *Phys. Rev. Lett.* **45**, 144–147.
- Dorch, S.B.F. & Archontis, V. 2004 On the saturation of astrophysical dynamos: numerical experiments with the no-cosines flow. *Solar Phys.* **224** 171–178. Referred to as DA in the text.

- Dombre, T. Frisch, U., Greene, J.M., Hénon, M., Mehr, A. & Soward, A.M. 1986 Chaotic streamlines in the ABC flows. *J. Fluid Mech.* **167**, 353–391.
- Friedlander, S. & Vishik, M.M. 1995 On stability and instability criteria for magnetohydrodynamics *Chaos* **5**, 416–423.
- Galloway, D.J. & Proctor, M.R.E. 1992 Numerical calculations of fast dynamos in smooth velocity fields with realistic diffusion. *Nature* **356**, 691–693.
- Gilbert, A.D. 1992 Magnetic field evolution in steady chaotic flows. *Phil. Trans. R. Soc. Lond. A* **339**, 627–656.
- Ladyzhenskaya, O.A. 1969 *The mathematical theory of viscous incompressible flow*. Gordon and Breach, New York, London.
- Leray, J. & Schauder, J. 1934 Topologie et equations fonctionnelles. *Ann. Sci. École Norm. Sup.* **13**, 45–78.
- Mason, J., Cattaneo, F. & Boldyrev, S. 2006 Dynamic alignment in driven magnetohydrodynamic turbulence *Phys. Rev. Lett.* **97**, 255002.
- Pouquet, A., Meneguzzi, M. & Frisch, U. 1986 Growth of correlations in magnetohydrodynamic turbulence *Phys. Rev. A* **33**, 4266–4276.
- Sur, S. & Brandenburg, A. 2009 The role of the Yoshizawa effect in the Archontis dynamo. *Mon. Not. R. Astron. Soc.* **399**, 273–280.
- Taylor, M. 1981 *Pseudodifferential operators*. Princeton University Press.
- Zheligovsky, V. 2009 Determination of a flow generating a neutral magnetic mode. *Phys. Rev. E*, **80**, 036310.
- Zheligovsky, V. 2010 A priori bounds for Gevrey–Sobolev norms of space-periodic three-dimensional solutions to equations of hydrodynamic type. *Differential and integral equations*, submitted (arXiv:1001.4237 [math.AP]).
- Zienicke, E., Politano, H. & Pouquet, A. 1998 Variable intensity of Lagrangian chaos in the nonlinear dynamo problem. *Phys. Rev. Lett.* **81**, 4640–4643.